

Figure 4. Trailed spectrograms (top panels), Doppler maps (middle panels) and computed data (bottom panels) are plotted for $H\beta$, $He\ II\ 4686\ \text{\AA}$, and $He\ I\ 4472\ \text{\AA}$ for both nights. The computed data were reconstructed from the Doppler maps. The letters A, B and C mark flares visible in both $H\beta$ and $He\ II\ 4686\ \text{\AA}$; these lead to some artifacts (diagonal stripes) in the maps.

Spiral structure in IP Pegasi; how persistent is it?

L. Morales-Rueda¹, T. R. Marsh¹ and I. Billington²

¹*Dept of Physics and Astronomy, Southampton University, (lmr@astro.soton.ac.uk, trm@astro.soton.ac.uk)*

²*Swiss Bank Corp., City of London*

Accepted ... Received ...; in original form ...

ABSTRACT

We present spectroscopy of the dwarf nova IP Pegasi taken during two consecutive nights, 5 and 6 days after the start of an outburst. Even this late in the outburst, Doppler maps show marked spiral structure in the accretion disc, at least as strongly as seen earlier in other outbursts of IP Peg. The spiral shocks are present on both nights with no diminution in strength from one night to the next. The light curves of the lines show an offset to earlier phases, with the mid-eclipse of the emission lines displaced to phases between -0.015 ± 0.001 and -0.045 ± 0.009 . This cannot be explained by the presence of the accretion shocks. As well as the fixed spiral pattern, the disc shows strong flaring in the Balmer and He II $\lambda 4686$ Å lines. Irradiation-induced emission is seen from the companion star in the Balmer, He I, He II, Mg II, C II, and other lines. The emission is located near the poles of the companion star, suggesting that the accretion disc shields the companion star substantially and thus has an effective H/R of order 0.2 at EUV wavelengths. The Balmer emission is distinctly broader than the other lines consistent with non-Doppler broadening.

Key words:

accretion, accretion discs – binaries: spectroscopic – line: profiles – stars: mass-loss – stars: novae, cataclysmic variables – stars: individual: IP Peg.

1 INTRODUCTION

IP Peg is an eclipsing cataclysmic variable (CV) of period 3.8 hours (Wolf et al. 1993) that shows dwarf nova outbursts approximately every 3 months. During these high states, which last about 12 days, the system goes from V magnitude 15 to 12. IP Peg has received much publicity recently as it was found to show strong spiral structure in the accretion disc during outburst (Steeghs, Harlaftis & Horne 1997; Harlaftis et al. 1999). Spiral shocks generated by tidal forces from the companion star, were proposed as a possible mechanism of angular momentum transport by Sawada, Matsuda & Hachisu (1986) and Spruit et al. (1987), but had never been observed until Steeghs et al.’s work. The spiral pattern seems to be present only during outburst, consistent with the idea that, to avoid producing too tightly wound a spiral, the gas in the disc must have low Mach number (i.e. the speed of the flow is not very large compared with the speed of sound in the disc). Two other systems that possibly show signs of spiral shocks in their accretion discs are SS Cyg (Steeghs et al. 1996) and EX Dra (Steeghs priv. comm.).

In the standard disc instability model of dwarf nova outbursts, the viscosity in the disc increases significantly as the disc makes the transition to outburst. This will drive the disc outwards against the tidal field of the companion star which truncates the disc. It is at this point that one ex-

pects the spiral shocks to develop. However, it is not known yet how the spiral structure evolves with time or if it is present in every outburst, therefore observations of the outbursts at all epochs are of interest. The detections by Steeghs et al. (1997) and Harlaftis et al. (1999) were made 1.5 and 3 days after the start of the August 1993 and the November 1996 outbursts respectively, whereas spectroscopic data taken 8 days after the start of the August 1993 outburst by Steeghs et al. (1996) only hints at their presence. In this paper, we present data taken on two nights, 5 and 6 days after IP Peg went into outburst in August 1994. This covers times intermediate between phases when the spiral structure is seen strongly, and when it is difficult to detect. We report the presence of strong spiral structure in the accretion disc on both nights. We also detect the effect of spiral structure upon the emission line eclipse light curves, and shielding of the companion star by the disc.

We start by describing the observations, and then present our results and conclusions.

2 OBSERVATIONS

We obtained spectrophotometry of IP Peg on the nights of 1994 August 30 and 31, 5 and 6 nights after the start of an outburst, using the Intermediate Dispersion Spectrograph

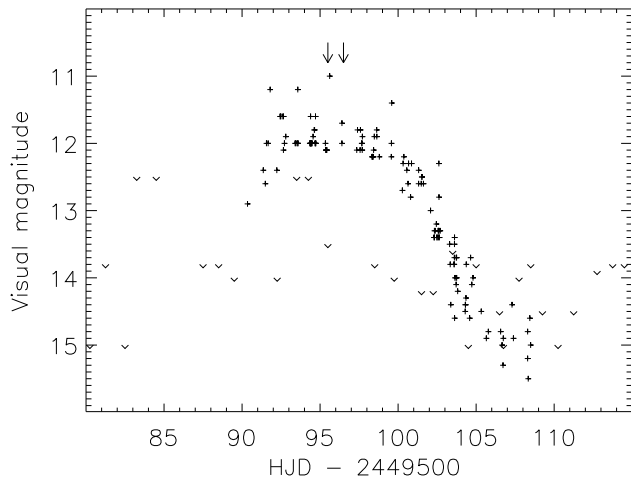


Figure 1. The visual light curve of IP Peg during the August 1994 outburst obtained from the American Association of Variable Star Observers (<http://www.aavso.org/>). The arrows indicate the times of our spectrophotometric observations.

Table 1. Journal of observations. E is the cycle number plus binary phase with respect to the ephemeris given by Wolf et al. (1993). Phases have been adjusted by 0.043 so that phase 0 corresponds to superior conjunction of the white dwarf.

Date (1994 Aug)	Start (UT)	End (UT)	Start ($E - 2500$)	End ($E - 2500$)	No. of spectra
30	1.48	5.99	158.004	159.193	69
31	23.66	6.08	163.844	165.536	95

mounted on the 2.5 m Isaac Newton Telescope (INT) on La Palma. Table 1 gives a journal of observations; Fig. 1 shows a visual light curve obtained by the American Association of Variable Star Observers (AAVSO) during the August 1994 outburst, with arrows indicating the days on which we made observations. The standard readout mode was used in conjunction with a Tektronix CCD windowed to 1024×90 pixels to reduce dead time. Exposure times were generally 150 s, with ~ 70 s dead time, and the spectral resolution corresponds to 100 km s^{-1} at $H\beta$. The 1200 lines mm^{-1} grating R1200Y was used to cover the wavelength range $\lambda\lambda 4040 - 4983 \text{ \AA}$ enabling simultaneous monitoring of $H\beta$, $H\gamma$ and $\text{He II } \lambda 4686 \text{ \AA}$. A total of 164 usable spectra were obtained.

After debiasing and flat-fielding the frames by tungsten lamp exposures, spectral extraction proceeded according to the optimal algorithm of Horne (1986). The data were wavelength calibrated using a CuAr arc lamp and corrected for instrumental response and extinction using the flux standard HD 19445 (Oke & Gunn 1983). The spectrograph slit orientation allowed a nearby star to be employed as calibration for light losses on the slit.

3 RESULTS

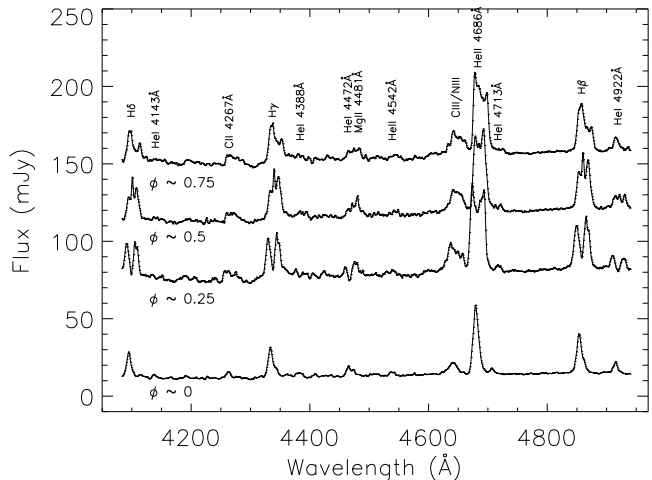


Figure 2. Spectra of IP Peg taken during outburst. The spectra are binned into 4 orbital phase slots. An offset of 40 mJy was included between consecutive spectra for display purposes.

3.1 Average spectra

The average spectra of IP Peg during outburst shows Balmer, He I and He II as well as some Mg II, C II, C III and N III emission lines on a blue continuum. The lines appear double-peaked during most orbital phases. Fig. 2 shows the spectra of IP Peg for 4 different orbital bins where the changes of the line profiles are clear. Harlaftis (1999) presents outburst spectra of IP Peg at a slightly different wavelength range where Ti II emission lines are also present.

3.2 Doppler maps

We use the maximum entropy method (MEM) to construct velocity maps of IP Peg in different emission lines. Fig. 3 shows the images in the light of $\text{He II } \lambda 4686 \text{ \AA}$, and demonstrates the presence of strong spiral structure on each night, with little, if any, change from night to night. There is also some emission near the secondary star. This spiral structure has previously been observed in IP Peg 1.5 days and possibly 8 days after the start of the August 1993 outburst by Steeghs et al. (1996, 1997, 1998), and 3 days after the start of the November 1996 outburst by Harlaftis et al. (1999); the spectra taken 8 days after the start of the August 1993 outburst only hint at the presence of the spiral shocks. The data presented in this paper fit in nicely between the previous observations and have the extra advantage that, for the first time, were taken for two consecutive nights during an outburst. We see that the spiral structure is strong both nights and with little alteration which indicates that the time-scale of the duration of the spiral shocks is of the order of days instead of hours. As already mentioned, the data presented in this paper were taken 5 and 6 days after the outburst had started, indicating that the spiral shocks are long-lived structures that are probably present throughout the entire outburst although we cannot be certain until spectroscopy for the entire duration of an outburst is obtained.

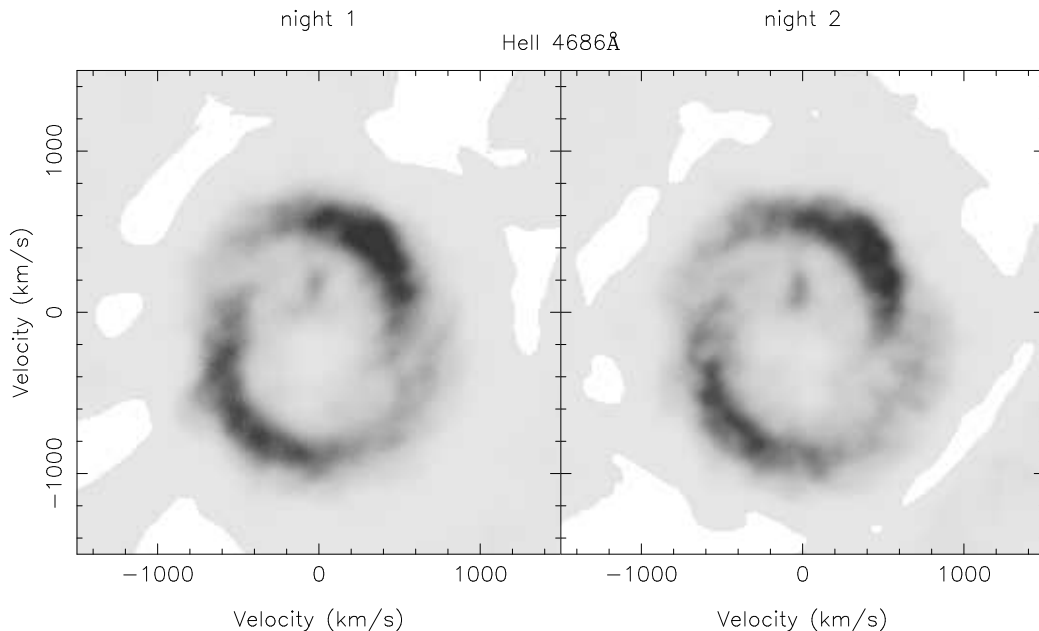


Figure 3. Doppler maps of He II $\lambda 4686 \text{ \AA}$ for both nights of observations obtained using the MEM mapping technique.

Fig. 4 compares maps of different emission lines ($H\beta$, He II $\lambda 4686 \text{ \AA}$ and He I $\lambda 4472 \text{ \AA}$) and also displays the data (top panels) and fits (lower panels). To construct these maps (and those of Fig. 3) the eclipse data have been removed as the behaviour during eclipse is not included in the model. The spiral structure is strongest in He II $\lambda 4686 \text{ \AA}$ whereas both $H\beta$ and He I $\lambda 4472 \text{ \AA}$ feature very strong emission from the companion star. The He I $\lambda 4472 \text{ \AA}$ image is distinctly different in structure with the upper shock stronger than the lower. This may be associated with its weakness; for instance in computing this map we had to simultaneously calculate one for the nearby Mg II $\lambda 4481 \text{ \AA}$ line. The upper shock in the He I $\lambda 4472 \text{ \AA}$ maps shows a more complex structure than that of the other lines. This structure is seen in maps from both nights, which suggests that it is real. As for $H\beta$, the brightest region on the upper shock is shifted in azimuth with respect to He II $\lambda 4686 \text{ \AA}$.

3.3 Flares

There are substantial flares in the emission lines, e.g. in $H\beta$ and He II $\lambda 4686 \text{ \AA}$ at orbital phase ~ 1.3 during the first night.

We have labelled some of the flares in the trailed spectra (top panels) of $H\beta$ and He II $\lambda 4686 \text{ \AA}$ in Fig. 3.2. The flare events, which last for one or two spectra (i.e. a few minutes), are clear in both lines and occur in both the blue- and red-shifted sides of the lines. Flares A and B occur at high radial velocities in the blue-shifted component. Label C is associated with a flare that took place in the red-shifted component of the lines.

3.4 Continuum and emission lines eclipses

The continuum and emission line fluxes for the two nights are plotted versus orbital phase in Fig. 5. Orbital phases

Table 2. Phases of mid-eclipse.

Emission line	Phase of mid-eclipse
$H\gamma$	-0.030 ± 0.003
$H\beta$	-0.029 ± 0.004
He I $\lambda 4472 \text{ \AA}$	-0.045 ± 0.009
He II $\lambda 4686 \text{ \AA}$	-0.015 ± 0.001
Continuum	-0.006 ± 0.003

have been calculated using Wolf et al.’s (1993) linear ephemeris:

$$T_0(HJD) = 2445615.4156 + 0.15820616E \quad (1)$$

The shape of the continuum eclipses is similar to that of He II $\lambda 4686 \text{ \AA}$ whereas the shape of the eclipses for the other lines is quite different. They are more asymmetric and show a slope shallower than that of He II $\lambda 4686 \text{ \AA}$ and the continuum during both ingress and egress. The eclipse of the emission lines is shifted to earlier-than-expected phases; the continuum is too, but to a lesser extent. The shift in phase is different for different lines being the largest displacement that of He I $\lambda 4472 \text{ \AA}$ which we singled out earlier for its asymmetry. The phases of mid-eclipse measured at half eclipse depth are listed in Table 2 during eclipse. Another feature of these light curves is the variability observed between eclipses with a double-hump in the Balmer and He I $\lambda 4472 \text{ \AA}$ lines. This double-hump behaviour is also seen during the September 1997 outburst in the infrared (Webb 1999) and may result from shadowing by the spiral shocks (Steehgs priv. comm.). Adding the quadratic term of the ephemeris (as given by Wolf et al. 1993) results in an orbital phase change of ~ 0.006 which cannot explain the shifts observed in the eclipses of the emission lines.

By assuming a Keplerian accretion flow we transform the velocity coordinates of the Doppler maps to space co-

Landscape figure to go here.

Figure 4.

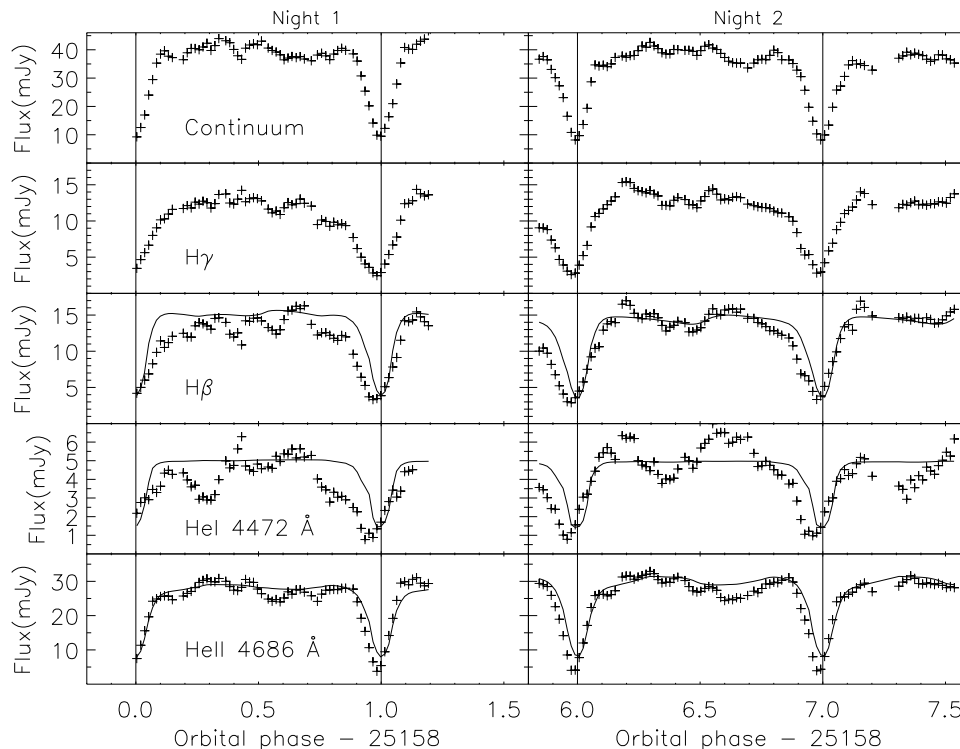


Figure 5. Light curves of the continuum, $H\gamma$, $H\beta$, $\text{He I } \lambda 4472 \text{ \AA}$, and $\text{He II } \lambda 4686 \text{ \AA}$ obtained during both nights. The model light curves for $H\beta$, $\text{He I } \lambda 4472 \text{ \AA}$, and $\text{He II } \lambda 4686 \text{ \AA}$ are over plotted to the data.

ordinates and compute model spectra for $H\beta$, $\text{He II } \lambda 4686 \text{ \AA}$, and $\text{He I } \lambda 4472 \text{ \AA}$. These spectra, shown in the lower panels of Fig. 4, are calculated at all orbital phases, including during eclipse. Although the spectra during the eclipse were not used to obtain the Doppler images, we can calculate the computed spectra during eclipse. These spectra can be calculated from the maps by using IP Peg’s parameters, given by Marsh & Horne (1990). The translation from velocities to positions becomes doubtful at low velocities which can end outside the Roche lobe. We arbitrarily decided to ignore any eclipse of points which mapped to locations beyond $r = R_{L1}$. The light curves generated from the computed and real data are plotted in Fig. 5 with solid lines and crosses respectively. The eclipses of the computed and real data do not occur at the same time. The model data do not show the shift of minimum light towards earlier orbital phases displayed by the data. Shifts of the sort seen in the data require a large asymmetry in the emission line flux distribution about the line of centres of the two stars. The spiral shocks do have this asymmetry but apparently not large enough to explain the shifts that we see. We have no plausible explanation for this.

3.5 Companion star

We noticed in section 3.2 that the secondary star contributed to the Balmer emission and almost none of the $\text{He II } \lambda 4686 \text{ \AA}$ emission. In the top panels of Fig. 6, we show the Doppler maps obtained from the combined spectra for both nights but this time centered and expanded around the secondary star instead of the centre of mass of the system. The symmetric component of the accretion disc for $\text{He II } \lambda 4686 \text{ \AA}$ has

been subtracted and the saturation levels on the map adjusted to emphasize the companion star. The ratio of the masses of both components used is $q = 0.49$ and the radial velocity semi-amplitude of the secondary $K_2 = 300 \text{ km s}^{-1}$ (Marsh & Horne 1990). Maps for the Balmer lines, He II , He I , Mg II , and C II are shown. We also find significant emission coming from the red star at wavelengths: 4126.5 \AA , 4132.5 \AA , 4271.7 \AA , 4383.6 \AA , 4442.4 \AA , 4507.8 \AA , 4548.9 \AA , 4823.4 \AA , and 4890.8 \AA . We used an LTE model of gas combined with the atomic spectral line list of Hirata & Horaguchi (1995) at temperatures between 3000 and 15000 K but were unable to identify these lines. To discard the possibility of the lines being the result of high ionisation, we also compared them with emission lines observed in planetary nebulae without success.

We see that the Balmer emission is more spread on the surface of the secondary star than any of the other emission lines. This effect, already observed in post-common envelope binaries like GD 448 (Maxted et al. 1998), RE 1016–053 and RE 2013+400 (Wood, Harmer & Lockley 1999) has been explained as the result of the Balmer lines being intrinsically broadened due to optical depth effects; this is clear evidence that the same effect appears in CVs. Therefore the width of the Balmer lines is not a reliable indication of their spatial distribution.

The position of the irradiated region on the companion star seems to vary from line to line but most importantly, it is located between the inner Lagrangian point and the pole of the secondary for all emission lines except perhaps He II . We tested for the effect of noise by generating artificial Doppler maps with noise equivalent to that in our data; these data showed that the noise does not cause significant

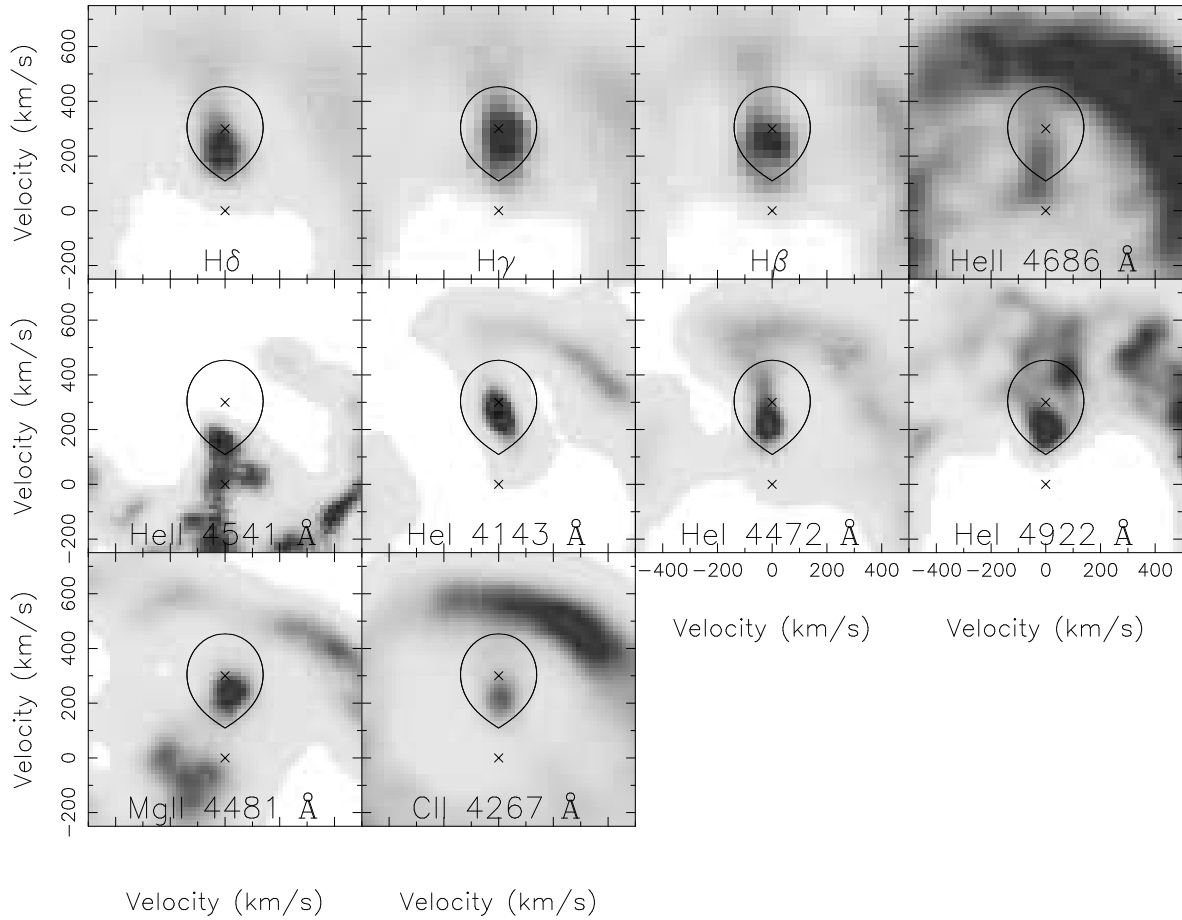


Figure 6. Doppler maps in the region of the secondary star in IP Peg for different emission lines. The Roche lobe of the secondary star, and two crosses indicating the centre of the secondary star and the centre of mass of the system are also plotted.

shifts in the location of the irradiated spot. The presence of an irradiation spot on the surface of the companion star would produce a very clear signature in its light curve, unfortunately due to the complexity of the spectra it is difficult to extract a light curve with only the contribution from the secondary star. However, we can see flux modulated with the companion’s motion in the trailed spectra shown in Fig. 4 indicating the presence of such an irradiated region near the inner Lagrangian point. We believe that this behaviour is a consequence of irradiation of the companion by the inner disc and white dwarf under the influence of shadowing by the disc. Fig. 7 shows an edge-on view of IP Peg assuming that the disc is thick enough to shield the companion almost entirely.

Only a region near the poles of the companion star can see the inner disc and white dwarf, and therefore we expect to see emission displaced from the L1 point towards the centre of mass of the secondary star. This displacement survives the process of Doppler tomography, even though it does not strictly satisfy the assumptions which underly it: in Fig. 8 we show maps derived taking shadowing and Roche lobe geometry into account for $H/R = 0.0, 0.15,$ and 0.30 (any-

thing larger than 0.31 prevents all light from reaching the secondary star). Comparing this figure with the real maps, suggests that the disc has an effective $H/R \approx 0.2$. The H/R may be able to vary owing to wavelength-dependent opacity at the EUV wavelengths appropriate for photoionisation of the various species involved. For instance, the Balmer lines require photons with $h\nu > 13.6$ eV, compared to 24 eV for He I $\lambda 4472$ Å and 54 eV for He II $\lambda 4686$ Å. We would expect the opacity at 13.6 eV to be largest (because of neutral hydrogen), and thus the disc to appear thickest for the Balmer lines. Our data are suggestive of this effect, although not conclusive. Higher resolution observations would be of use because apart from the Balmer emission, the irradiated features are not resolved in our data.

4 CONCLUSIONS

We have discovered spiral shocks in the August 1994 outburst of the dwarf nova IP Peg 5 and 6 days after the system went into outburst and with no noticeable diminution in strength from one day to the next. Our data extend the duration over which spiral structure is known to remain

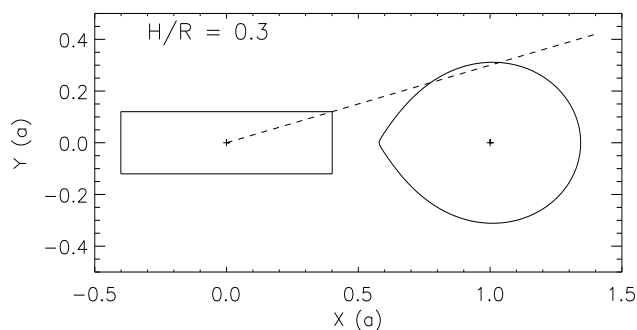


Figure 7. An edge-on view of IP Peg showing how the disc can shadow the equator of the secondary star. For this plot we have chosen $H/R = 0.3$.

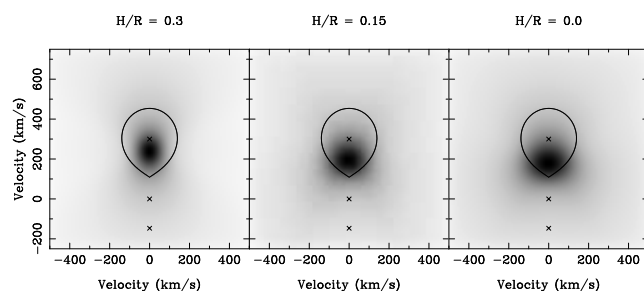


Figure 8. Simulated irradiation pattern on the surface of the red star for three different disc thicknesses, $H/R = 0.0$ (left), 0.15 (centre), and 0.30 (right). The Roche lobe of the companion star is also plotted in all maps to help identify the position of the irradiated region. The centre of mass and the position of the white dwarf are marked with a cross.

strong, and suggest that they could last the entire outburst. The eclipses of the emission lines are shifted by about 0.015 – 0.045 towards earlier phases than that of the white dwarf. These shifts towards earlier phases require a large-scale asymmetry about the line of centres of the two stars larger than the spiral shocks suggest. We cannot explain this. The disc is also apparently variable on short timescales as we see several strong flares in both Balmer and He II emission lines.

Doppler maps of line emission on the companion star show that it is located between the inner Lagrangian point and the poles of the star, and that it avoids the equator. This is strong evidence for shielding of the companion star by the disc. From comparison with models, the shielding must be substantial, requiring a height-to-radius ratio in the disc of $H/R \approx 0.2$. There is some evidence for variability in the location of the emission, as might be expected if the disc appears to vary in thickness according to the threshold wavelength needed to drive the respective emission line. The Balmer emission from the companion is clearly broader than the other emission lines, supporting evidence from detached binaries for non-Doppler broadening in this line.

Acknowledgments

The Isaac Newton Telescope is operated on the island of La Palma by the Isaac Newton Group in the Spanish Observatorio del Roque de los Muchachos of the Instituto de Astrofísica de Canarias. In this research, we have used, and acknowledge with thanks, data from the AAVSO International Database, based on observations submitted to the AAVSO by variable star observers worldwide. The reduction and analysis of the data were carried out on the Southampton node of the STARLINK network. LM-R wishes to thank L. González Hernández for computer support.

REFERENCES

- Harlaftis E., 1999, *A&A*, 346, L73-L75
 Harlaftis E. T., Steeghs D., Horne K., Martín E., Magazzú A., 1999, *MNRAS*, 306, 348
 Hirata R., Horaguchi T., 1995, <http://cdsweb.u-strasbg.fr/cgi-bin/Cat?VI/69>
 Horne K., 1986, *PASP*, 98, 609
 Marsh T. R., Horne K., 1990, *ApJ*, 349, 593-607
 Maxted P. F. L., Marsh T. R., Moran C., Dhillon V. S., Hilditch R. W., 1998, *MNRAS*, 300, 1225
 Oke J. B., Gunn, J. E., 1983, *ApJ*, 266, 713
 Sawada E., Matsuda T., Hachisu I., 1986, *MNRAS*, 219, 75
 Spruit H. C., Matsuda T., Inoue M., Sawada K., 1987, *MNRAS*, 229, 517
 Steeghs D., Harlaftis E. T., Horne K., 1997, *MNRAS*, 270, L28
 Steeghs D., Harlaftis E. T., Horne K., 1998, *MNRAS*, 296, 463-464
 Steeghs D., Horne K., Marsh T. R., Donati J. F., 1996, *MNRAS*, 281, 626-636
 Webb N., 1999, *Proceedings of the Symposium in honour of Brian Warner*, Eds. P. Charles, A. King, D. O'Donoghue, *in press*
 Wolf S., Mantel K. H., Horne K., Barwig H., Schoembs R., Baerbantner O., 1993, *A&A*, 273, 160-168
 Wood J. H., Harmer S., Lockley J. J., 1999, *MNRAS*, 304, 335